Hindawi
Mathematical Problems in Engineering
Volume 2020, Article ID 9685482, 14 pages
https://doi.org/10.1155/2020/9685482

Research Article

Analysis of MHD Fluids around a Linearly Stretching Sheet in Porous Media with Thermophoresis, Radiation, and Chemical Reaction

K. Jabeen, M. Mushtaq, and R. M. Akram Muntazir

Department of Mathematics, University of the Engineering and Technology, Lahore-54890, Pakistan

Correspondence should be addressed to K. Jabeen; kanwaljabeen44@yahoo.com

Received 28 February 2020; Accepted 17 April 2020; Published 7 May 2020

Academic Editor: Alessandro Mauro

This paper presents the comparative analysis of MHD boundary layer fluid flow around a linearly stretching surface in the presence of radiative heat flux, heat generation/absorption, thermophoresis velocity, and chemical reaction effects in a permeable surface. The governing equations are highly nonlinear PDEs which are converted into coupled ODEs with the help of dimensionless variables and solved by using semianalytical techniques. The numerical and graphical outcomes are observed and presented via tables and graphs. Also, the Nusselt and Sherwood numbers and skin friction coefficient are illustrated by tables. On observation of heat and mass transfer, it was noticed that Maxwell fluid dominates the other fluids such as Newtonian, Williamson, and Casson fluid due to high rate of thermal conductivity, and hence, Maxwell fluid has better tendency for heat and mass transfer than other Newtonian and non-Newtonian fluids.

1. Introduction

There exist different types of fluids in nature such as water, oil, alcohol, glycerine, gasoline, polymer melts, colloidal suspension, condensed milk, ketchup, clay, paints, slurries, gels, drilling muds, toothpaste, mayonnaise, cheese, blood, and printer ink. Some of them are the fluids that obey Newton's viscosity law and are dropped in the category of Newtonian fluids because in them, the relationship of viscosity is constant with shear rate. But, some of the fluids have nonlinear viscosity interaction with shear rate, so those fluids are referred as non-Newtonian fluids. The governing non-Newtonian fluid equations are highly nonlinear and complex in nature; thus, due to the complexity, the single Navier–Stokes relation is not enough to handle all the rheological properties of non-Newtonian fluids. To overcome this deficiency, further, the non-Newtonian fluids are classified into three basic categories:

(i) The differential type

(ii) The rate type

(iii) The integral type

As a fluid is incapable of representing the entire properties of flow behavior in a single model, therefore, non-Newtonian fluids are distinguished by individual models such as Maxwell (1867), Barus (1893), Jaffrey (1915), Bingham (1922), power law (1923), Williamson (1929), Eyring–Powell (1936), Burger (1939), generalized Burger (1939), Oldroyd-A (1950), Oldroyd-B (1950), Oldroyd-8 constant (1950), Sisko (1950), Casson (1959), Cross (1965), Carreau (1972), and Carreau–Yasuda (1972). Due to vital applications of non-Newtonian fluids in the industrial and engineering field, researchers and scientists have taken much interest in non-Newtonian fluids and developed a number of fluid models in which some of the models are empirical and some are semiempirical. Also, some of the proposed models which are presented in nature do not agree with experiments due to their complex structures. So, the closed form solutions do not exist with practical concerns. Hence, semi-empirical equations have been invoked. Due to multiple characteristics, Casson, Maxwell, and Williamson fluids have their own importance in the literature.

Other well-known rate-type fluid is Maxwell's fluid. This simplest viscoelastic fluid was firstly proposed by Maxwell in 1867. By this special type of the fluid model, relaxation time effects can be counted.

The decreasing direction of thermal gradient movement of small particles is referred as thermophoresis of particles. Simply, one can say thermophoresis helps to gather the small particles on the less heated or cold surface. By Aitken's phenomenon, the molecules of the gas have greater velocity of migration from the hot region when compared with the velocity of migrated molecules from the cold region. The faster moving molecules have intensity to collide more forcefully with the particles. So, this attained velocity by the particles is called thermophoresis velocity, while due to thermal gradient, the force which is endured by the particles is called thermophoretic force which is opposite to the direction of temperature gradient.

Hayat and Qasim and Noor had investigated the influences of chemical reaction and thermophoresis along a vertical stretching sheet of MHD Maxwell fluid flow [1, 2]. In 2013, Stanford also studied MHD Maxwell fluid flow by considering the effects of thermophoresis and chemical reaction and concluded that the newly developed scheme discussed in their work has an ability to solve nonlinear coupled ODEs [3]. Hayat et al. discussed the non-Newtonian fluid in the porous medium with heat source/sink properties and found the dual solutions for momentum and thermal profiles [4]. Heat and mass transfer analysis with chemically reacting MHD non-Newtonian fluids such as Casson and Maxwell was theoretically investigated by Abbasi and Shehzad [5].

The effects of three-dimensional MHD upper convected Maxwell fluid with joule heating, viscous dissipation, and thermophoresis velocity on heat and mass transfer analysis [6] were studied by Bilal et al., and they presented the comparison of Maxwell fluid with Newtonian fluid [7]. Thermophysical properties on viscoelastic fluids over a vertical surface were investigated by Koriko et al. [8] with nth order of chemical reaction. Comparative analysis on behavior of Maxwell, Oldroyd-B, and Jeffrey nanofluids was discussed by Sandeep, in which they flow around a stretching surface with heat source/sink [8–10].

The other type of non-Newtonian fluid is Williamson fluid suggested by Williamson in 1929. The texture of the fluid model enlightened the shear thinning behavior of non-Newtonian fluids. The flow model is viscoinelastic, i.e., the fluid containing both viscous and elastic properties. Recently, many researchers considered MHD Williamson fluid [10–12] and analyzed the effects of thermophoresis velocity, heat source/sink, thermal radiation, and ohmic dissipation. [13–16]. Also, the comparative study of various fluids which was considered upon a permeable stretching sheet was discussed by Parmar and Jain, Kumar et al., and Raju et al. [14–16].

A well-known fluid having pseudo-plastic phenomenon is Casson fluid which was recommended by Casson in 1959. This fluid has shear thinning properties with high shear viscosity and yield stress. Human blood, honey, concentrated juices, ketchup, jelly, etc., are some common examples of Casson fluid [17–19]. In numerous areas of biotechnology, thermal engineering, geophysics [20, 21] and as well as astrophysical studies, heat and mass transfer in various non-Newtonian fluids has been fascinated by researchers and scientists because of its fruitful applications in multiple fields [21].

MHD two-dimensional and three-dimensional Casson fluid flow on a shrinking/stretching sheet [18–21] was studied by many researchers. Sumalatha and Bandari [22] analyzed the heat source/sink variations on a Casson fluid over a nonlinear stretched surface and concluded that by increasing radiation and heat source/sink parameter, the temperature of the fluid enhances.

Latter, researchers focused on the MHD Casson flow and discussed the effects of various physical parameters [23–25]. MHD Casson fluid with slip boundary on a moving edge was analyzed by Raju and Sandeep [26] and found dual solutions for accelerating and decelerating flow.

The purpose of the current study is to discuss the comparative impact of MHD flow [27–30] of Newtonian, Maxwell, Williamson, and Casson fluids under the effects of internal heat source/sink, thermal radiation, chemical reaction, and thermophoretic velocity [31–36] on the momentum and heat and mass transfer over a stretching sheet with permeability effects [37–41].

The problem is considered under the following conditions:

(i) $\beta = \infty$, $\lambda = 0$, and $We = 0$. The problem falls in the Newtonian fluid category.

(ii) $\beta = \infty$, $\lambda \neq 0$, and $We = 0$. The problem follows the Maxwell fluid.

(iii) $\beta = \infty$, $\lambda = 0$, and $We \neq 0$. The problem represents the Williamson fluid.

(iv) $\beta \neq 0$, $\lambda = 0$, and $We = 0$. The problem depicts the Casson fluid.

2. Mathematical Formulation

We have considered the steady-state two-dimensional flow of viscous incompressible fluids. The flow is taken into account at various situations of fluid behavior caused by the linearly stretched sheet having stretching velocity $u_w = ax$, where a is a +ive constant. Also, T_w and C_w are the fluid's temperature and concentration near the permeable stretched surface. With constant intensity B_o, magnetic field is applied in y direction. Temperature and concentration are considered in the direction of chemical reaction, thermal radiation, and thermophoretic velocity. The governing boundary layer equations are

$$\frac{\partial u}{\partial x}+\frac{\partial v}{\partial y}=0, \tag{1}$$

$$u\frac{\partial u}{\partial x}+v\frac{\partial u}{\partial y}+\lambda_1\left(u^2\frac{\partial^2 u}{\partial y^2}+v^2\frac{\partial^2 u}{\partial y^2}+2uv\frac{\partial^2 u}{\partial x\partial y}\right)=\left(1+\frac{1}{\beta}\right)\frac{\partial^2 u}{\partial y^2}+\sqrt{2}v\Gamma\frac{\partial v}{\partial y}\frac{\partial^2 u}{\partial y^2}-\frac{\sigma B_0^2}{\rho}u-\frac{v}{kp'}u, \tag{2}$$

$$u\frac{\partial T}{\partial x}+v\frac{\partial T}{\partial y}=\frac{k}{\rho C_p}\frac{\partial^2 T}{\partial y^2}+\frac{\mu}{\rho C_p}\left(\frac{\partial u}{\partial y}\right)^2+\frac{\sigma B_0^2 u^2}{\rho C_p}+\left(T-T_\infty\right)\frac{Q_0}{\rho C_p}-\frac{1}{\rho C_p}\frac{\partial q_r}{\partial y}+\frac{k}{\nu x\rho C_p}\left[\frac{u}{ax}A^*\left(T_w-T_\infty\right)-B^*\left(T-T_\infty\right)\right], \tag{3}$$

$$\begin{aligned}&u\frac{\partial C}{\partial x}+v\frac{\partial C}{\partial y}=D\frac{\partial^2 C}{\partial y^2}+D_m\frac{k_T}{T_m}\frac{\partial^2 T}{\partial y^2}-\frac{\partial\left(V_T\left(C-C_\infty\right)\right)}{\partial y}-k_1\left(C-C_\infty\right),\\&\begin{cases}y=0\text{: } u(x,0)=U_w=ax, & v(x,0)=-v_w, T=T_w, C=C_w,\\ y\longrightarrow\infty\text{: } u(x,y)\longrightarrow 0, & T\longrightarrow T_\infty, C\longrightarrow C_\infty.\end{cases}\end{aligned} \tag{4}$$

Here, the horizontal and vertical components of velocity u and v are in direction of x- and y-axis and β, λ and, We are the Casson, Maxwell, and Williamson parameters. The radioactive heating flux in the temperature equation is calculated and simplified by the Rosseland approximation, i.e.,

$$q_r=-\frac{4\sigma^*}{3k^*}\frac{\partial T^4}{\partial y}, \tag{5}$$

where σ^* is the Stefan–Boltzmann constant and k^* is the mean absorption coefficient.

The temperature variation within the flow is supposed to be small enough, so T^4 can be taken as a linear function of temperature neglecting the higher-order term while expanding T^4 in Taylor series about T_∞ which is obtained as [34]

$$T^4=T_\infty^4+4T_\infty^3\left(T-T_\infty\right)^2+6T_\infty^2\left(T-T_\infty\right)^2+\ldots. \tag{6}$$

Neglecting the higher-order terms of the above said statement beyond the first degree in the series, we get

$$T^4\cong 4TT_\infty^3-3T_\infty^3. \tag{7}$$

Also, V_T is the thermophoretic velocity, defined and expressed as $V_T=(\nu k_{ro}/T_{ro})$; here, T_{ro} is the reference temperature, and k_{ro} is the coefficient of thermophoretic velocity.

The model 8–10 is solved by using semianalytical techniques such as HAM [13], VIM [39, 40], and ADM [40] along with Pade approximation [39, 40]. These standard techniques are strongly effective, reliable, and convenient in the literature and can be applicable directly on linear and nonlinear equations. Although, for their closed form solution while dealing with the unbounded domain, the Pade approximation has been considered [39, 40].

Introducing the similarity transformation [14],

$$\left.\begin{aligned}&\eta(x,y)=\sqrt{\frac{a}{\nu}}y,\\&\psi(x,y)=xf(\eta)\sqrt{a\nu},\\&u=axf'(\eta),\\&v=-\sqrt{a\nu}f,\\&\theta(\eta)=\frac{T-T_\infty}{T_w-T_\infty},\\&\phi(\eta)=\frac{C-C_\infty}{C_w-C_\infty},\\&T_w=T_\infty+bx,\\&C_w=C_\infty+cx.\end{aligned}\right\} \tag{8}$$

The nonlinear coupled PDEs are transformed into ODEs by the help of dimensionless variables such as

$$\left(1+\frac{1}{\beta}\right)f'''+ff''-f'^2-\lambda\left(f^2f'''-2ff'f''\right)-(M+Kp)f'+Wef''f'''=0, \tag{9}$$

$$\left(1+\frac{4}{3}R\right)\theta''+Pr\left(f\theta'-f'\theta\right)+PrEc\left(f''^2+Mf'^2\right)+QPr\theta+A^*f'+B^*\theta=0, \tag{10}$$

Table 1: Comparison of skin friction coefficient, Nusselt number, and Sherwood number for Newtonian fluid for different values of auxiliary parameters.

M	Kp	s	Ec	R	Pr	A^*	B^*	K_2	Sr	Sc	τ	$-f''(0)$	$-\theta'(0)$	$-\phi'(0)$
0.5												1.358851773	0.478554119	0.6262152456
1												1.530604754	0.3905122564	0.5915366176
1.5												1.686053404	0.3217341878	0.5666264453
	0.5											1.358851773	0.478554119	0.6262152456
	1											1.530604754	0.4220039108	0.594560359
	1.5											1.68053404	0.3782540601	0.5727179692
		0.1										1.413363143	0.5081884233	0.6463054257
		0.2										1.358851773	0.478554119	0.6262152456
		0.3										1.307097282	0.4522305046	0.6072356892
			0.1									1.358851773	0.5735079222	0.6360554603
			0.2									1.358851773	0.478554119	0.6262152456
			0.3									1.358851773	0.3814938956	0.6159609328
				0.5								1.358851773	0.478554119	0.6262152456
				1								1.358851773	0.3932054790	0.6136600170
				1.5								1.358851773	0.3409595997	0.6063645038
					1							1.358851773	0.2005172126	0.5856196932
					2							1.358851773	0.478554119	0.6262152456
					3							1.358851773	0.6977754388	0.6600736652
						0.1						1.358851773	0.5151964969	0.6351787679
						0.2						1.358851773	0.478554119	0.6262152456
						0.3						1.358851773	0.4418517444	0.6212536760
							0.1					1.358851773	0.5342156819	0.6351787679
							0.2					1.358851773	0.478554119	0.6262152456
							0.3					1.358851773	0.4221843345	0.6168898751
								0.1				1.358851773	0.478554119	0.5806979856
								0.2				1.358851773	0.478554119	0.6262152456
								0.3				1.358851773	0.478554119	0.6726294719
									0.1			1.358851773	0.478554119	0.6412028069
									0.2			1.358851773	0.478554119	0.6262152456
									0.3			1.358851773	0.478554119	0.6112628818
										0.5		1.358851773	0.478554119	0.6262152456
										1		1.358851773	0.478554119	1.016542530
										1.5		1.358851773	0.478554119	1.345708949
											0.5	1.358851773	0.478554119	0.6262152456
											1	1.358851773	0.478554119	0.7207448762
											1.5	1.358851773	0.478554119	0.8167538284

Table 2: Comparison of skin friction coefficient, Nusselt number, and Sherwood number for Maxwell fluid for different values of auxiliary parameters.

M	Kp	s	Ec	R	Pr	A^*	B^*	K_2	Sr	Sc	τ	$-f''(0)$	$-\theta'(0)$	$-\phi'(0)$
0.5												1.353324280	0.4874191864	0.6278201412
1												1.521957583	0.3984838639	0.5934300419
1.5												1.675290777	0.3298050352	0.5685513366
	0.5											1.353324280	0.4874191864	0.6278201412
	1											1.521957583	0.4288171809	0.5961259590
	1.5											1.675290777	0.3850419870	0.5741031817
		0.1										1.422911261	0.5154658871	0.6456438194
		0.2										1.353324280	0.4874191864	0.6278201412
		0.3										1.289679068	0.4616353275	0.6105511196
			0.1									1.353324280	0.5735313850	0.6352587896
			0.2									1.353324280	0.4874191864	0.6278201412
			0.3									1.353324280	0.3945858897	0.6197828633
				0.5								1.353324280	0.4874191864	0.6278201412
				1								1.353324280	0.3960162055	0.6139385018
				1.5								1.353324280	0.3414734245	0.6059737269
					1							1.353324280	0.1975237050	0.5846586550

Table 2: Continued.

M	Kp	s	Ec	R	Pr	A^*	B^*	K_2	Sr	Sc	τ	$-f''(0)$	$-\theta'(0)$	$-\phi'(0)$
					2							1.353324280	0.4874191864	0.6278201412
					3							1.353324280	0.7386866419	0.6668115825
						0.1						1.353324280	0.5250386801	0.632836336
						0.2						1.353324280	0.4874191864	0.6278201412
						0.3						1.353324280	0.4498770528	0.6228334784
							0.1					1.353324280	0.5497377608	0.6376617879
							0.2					1.353324280	0.4874191864	0.6278201412
							0.3					1.353324280	0.4252649559	0.6177077170
								0.1				1.353324280	0.4874191864	0.5815616856
								0.2				1.353324280	0.4874191864	0.6278201412
								0.3				1.353324280	0.4874191864	0.6750311237
									0.1			1.353324280	0.4874191864	0.6432997685
									0.2			1.353324280	0.4874191864	0.6278201412
									0.3			1.353324280	0.4874191864	0.6125092369
										0.5		1.353324280	0.4874191864	0.6278201412
										1		1.353324280	0.4874191864	1.022485609
										1.5		1.353324280	0.4874191864	1.355332127
											0.5	1.353324280	0.4874191864	0.6278201412
											1	1.353324280	0.4874191864	0.7262603423
											1.5	1.353324280	0.4874191864	0.826256830

Table 3: Comparison of skin friction coefficient, Nusselt number, and Sherwood number for Williamson fluid for different values of auxiliary parameters.

M	Kp	s	Ec	R	Pr	A^*	B^*	K_2	Sr	Sc	τ	$-f''(0)$	$-\theta'(0)$	$-\phi'(0)$
0.5												1.278645309	0.5691877361	0.6391368929
1												1.429266480	0.4770060050	0.6011548440
1.5												1.565373274	0.4111873073	0.5735580926
	0.5											1.278645309	0.5691877361	0.6391368929
	1											1.429266479	0.5673153070	0.6101740706
	1.5											1.565373274	0.5658389845	0.5913279964
		0.1										1.308728536	0.6346217331	0.6702536078
		0.2										1.278645309	0.5691877361	0.6391368929
		0.3										1.244775264	0.4801609553	0.6095489748
			0.1									1.278645309	0.6023577008	0.6446163043
			0.2									1.278645309	0.5691877361	0.6391368929
			0.3									1.278645309	0.4716433515	0.6253855697
				0.5								1.278645309	0.5691877361	0.6391368929
				1								1.278645309	0.4322072171	0.622220513518
				1.5								1.278645309	0.3644814057	0.6140233817
					1							1.278645309	0.2124257796	0.5923898145
					2							1.278645309	0.5691877361	0.6391368929
					3							1.278645309	0.6611989010	0.6712717114
						0.1						1.278645309	0.6142435959	0.6451672300
						0.2						1.278645309	0.5691877361	0.6391368929
						0.3						1.278645309	0.5240139473	0.6331060526
							0.1					1.278645309	0.6789155726	0.6548554580
							0.2					1.278645309	0.5691877361	0.6391368929
							0.3					1.278645309	0.4740625485	0.6249977122
								0.1				1.278645309	0.5691877361	0.5928443088
								0.2				1.278645309	0.5691877361	0.6391368929
								0.3				1.278645309	0.5691877361	0.6862647508
									0.1			1.278645309	0.5691877361	0.6508951214
									0.3			1.278645309	0.5691877361	0.6391368929
									0.3			1.278645309	0.5691877361	0.6273310426
										0.5		1.278645309	0.5691877361	0.6391368929
										1		1.278645309	0.5691877361	1.051648397

Table 3: Continued.

M	Kp	s	Ec	R	Pr	A^*	B^*	K_2	Sr	Sc	τ	$-f''(0)$	$-\theta'(0)$	$-\phi'(0)$
										1.5		1.278645309	0.5691877361	1.404965985
											0.5	1.278645309	0.5691877361	0.6391368929
											1	1.278645309	0.5691877361	0.7341965506
											1.5	1.278645309	0.5691877361	0.8341420841

$$\phi'' + Sc\left(f\phi' - f'\phi\right) + ScSr\theta'' - ScK_2\phi - Sc\tau\left(\theta''\phi + \theta'\phi'\right) = 0, \tag{11}$$

Also, the transformed boundary conditions are

$$\begin{cases} f(0) = s; \\ f'(0) = 1; \\ f'(\infty) = 1; \\ \theta(0) = 1; \\ \theta(\infty) = 0; \\ \phi(0) = 1; \\ \phi(\infty) = 0. \end{cases} \tag{12}$$

Here, $M = (\sigma B^2/a\rho)$, and $kp = (\nu/akp')$ are the parameters of magnetic field and porosity.

$We = \Gamma x\sqrt{2a^3/\nu}$, $\lambda = a\lambda_1$, and β are the Williamson, Maxwell, and Casson fluid parameters. $Pr = (\mu C_p/k)$, $Ec = (a^2x^2)/(T_w - T_\infty)$, $Sc = (\nu/D)$, and $Sr = (D_m k_T/\nu T_m)$ $((T_w - T_\infty)/(C_w - C_\infty))$ are the Prandtl, Eckert, Schmidt, and Soret numbers, respectively. $Q = (Q_0/a\rho C_p)$ is the heat generation/absorption parameter, A^* and B^* are internal heat source/sink parameters, $R = (4\sigma^* T_\infty^3)/(k^* k)$ is the radiation parameter, $K_2 = (k_1/a)$ is the chemical reaction parameter, $V_T = (\nu k_r/T_r)(\partial T/\partial y)$ is thermophoretic velocity of the fluid, and $\tau = (\nu k_r/T_r)bx$ is the thermophoretic parameter.

3. Results and Discussion

In this part of the article, the observed consequences are exhibited graphically and numerically. For the pertinent values of physical parameters $M = Kp = R = Sc = \tau = 0.5$, $s = A^* = B^* = Ec = K_2 = Sr = 0.2$, $Q = 0$, and $Pr = 2$, the numerical and graphical solutions have been carried out for various situations of fluids. The effects of dimensionless parameters such as magnetic field (M), porosity parameter (Kp), suction/injection parameter (s) Eckert number (Ec), Prandtl number (Pr), heat source/sink parameter (A^*, B^*), radiation parameter (R), Schmidt (Sc), Soret numbers (Sr), thermophoretic velocity parameter (τ), and chemical reaction parameter (K_2) have been analyzed on the flow, heat and mass transfer of Newtonian, Maxwell, Williamson, and Casson fluids. Also, the effects of coefficient of skin friction, Nusselt, and Sherwood numbers are calculated and displayed via Tables 1–3. Figure 1 indicates the good agreement of analytical techniques.

Figures 2(a)–2(c) show the impact of magnetic field for multiple values of M. The graphs represent the behavior of Newtonian, Maxwell, Williamson, and Casson fluid. It was seen that the velocity profile for Casson fluid is highly affected by magnetic field in comparison with other fluids. Also, the momentum boundary layer thickness reduced while increasing this parameter M. This is because the fact when magnetic field is imposed in the $\perp$ direction on the electrically conducting fluid originate like the drag force (also named as Lorentz's force) that acts on the opposite direction of flow which hence produces a deceleration flow and causes the depreciation in the velocity profile. But, reverse effects are to be seen in case of thermal and concentration profiles. In them, we have seen the extreme behavior of Maxwell fluid by varying M.

It is obvious from Figures 3(a)–3(c) the behavior of porosity parameter Kp. It is observed that the velocity boundary layer decreases, and Casson fluid affects the most in this case. Generally, the porosity factor is responsible to soak the major amount of fluid from the boundary layer, so the velocity flow field decreases, but by increasing Kp amount, the thermal and concentration profiles increase, and Maxwell fluid is highly influenced than rest of the fluids under consideration.

Figures 4(a)–4(c) depict the behavior of suction parameter s for different fluids and boundary layer profiles. It is seen that all the profiles are decreasing, and Casson and Maxwell fluids in this situation are influenced highly by other Newtonian and non-Newtonian fluids. In fact, this trend of depreciating is pointing the physical situation of suction effect which is that it delays the separation and transition and helps to maintain the steady flow near the sheet. This observation indicates in Figure 3(a) that Casson fluid is more affected by increasing the values of s, while in Figures 4(b) and 4(c), it is seen that Maxwell fluid is extremely influenced by s.

The role of Eckert number on temperature profile $\theta(\eta)$ is observed in Figure 5(a). Physically, by upper-going values of Eckert number which tend to increase the thermal profile, the frictional heat generation is quite obvious as the fluid moves faster along the surface which causes the particles' growth of temperature. On comparison and analysis made by the graph, it can be observed that Maxwell fluid is more influenced than the other fluids.

It is evident from Figure 5(b) that the concentration profile is rapidly compressed by the destructive distillation parameter, i.e., chemical reaction. Because this appears with many instabilities, it results in high molecular motion and uplifts the transportation process and hence retards the fluid concentration. Also, it is interesting to note that Casson fluid shows more influenced in comparison with other fluids.

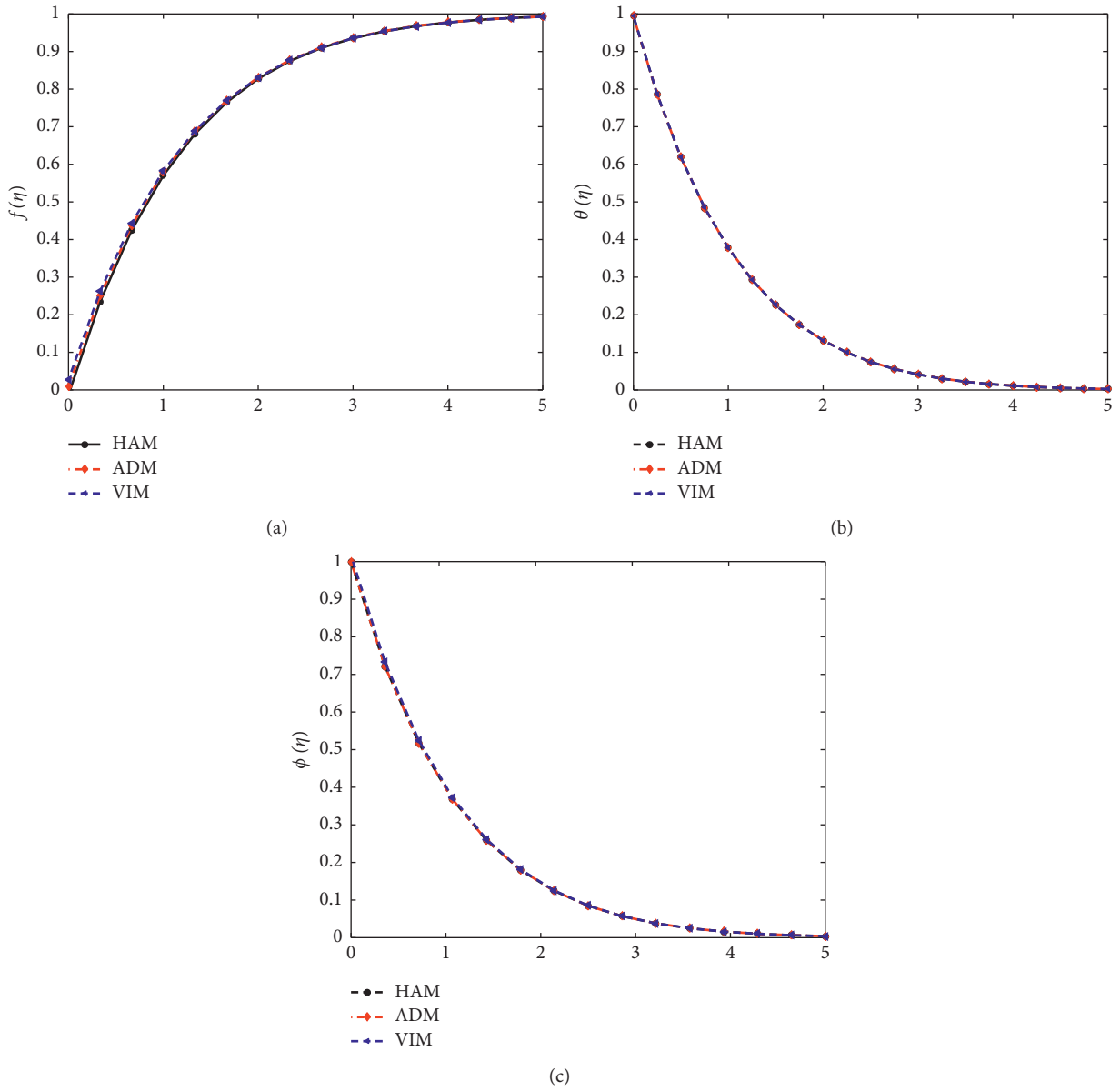

FIGURE 1: The comparison between HAM, ADM, and VIM for (a) $f(\eta)$, (b) $\theta(\eta)$, and (c) $\phi(\eta)$ when $\beta = \infty$, $\lambda = 0$, and $We = 0$, $M = Kp = R = Sc = \tau = 0.5$, $s = A^* = B^* = Ec = K_2 = Sr = 0.2$, $Q = 0$, and $Pr = 2$.

Behavior of Prandtl number is illustrated by Figure 6(a) with various fluid conditions. It is noticed that increasing Prandtl number causes decrement in the thermal layer, which is by the fact when thermal diffusivity decreases, the fluid temperature decreases because Prandtl's number is inversely proportional to thermal diffusivity, so it will lower the heat of the fluid for growing Pr. In Figure 6(b), it is clearly seen that Casson fluid is highly influenced as compared with other resting fluids.

By Figure 6(b), effects of thermomigration are successfully presented. From this figure, we can conclude that, by increasing the value of Soret number Sr, the concentration species rises in upward direction. Scientifically, transfer the mass flux from the lower to the maximum concentration region moved by the temperature gradient. Although all the Newtonian as well as non-Newtonian fluids' profiles are showing increasing behavior, Maxwell fluid is observed more influenced by other fluids.

It is noticed from Figure 7(a) that the radiation parameter R enlarges the temperature profile when the values of R increase. When the radiation effects exceed, the heat energy generates towards the flow which causes to elevate the heat, and hence, thermal profile proceeds. Maxwell fluid significantly affects much.

Figure 7(b) indicates the influence of Schmidt number. As the values increase, the concentration profile decreases due to the inverse relation between Sc and diffusion coefficient. The reason is that the mass transfer rate gets slower as we increase the diffusion coefficient.

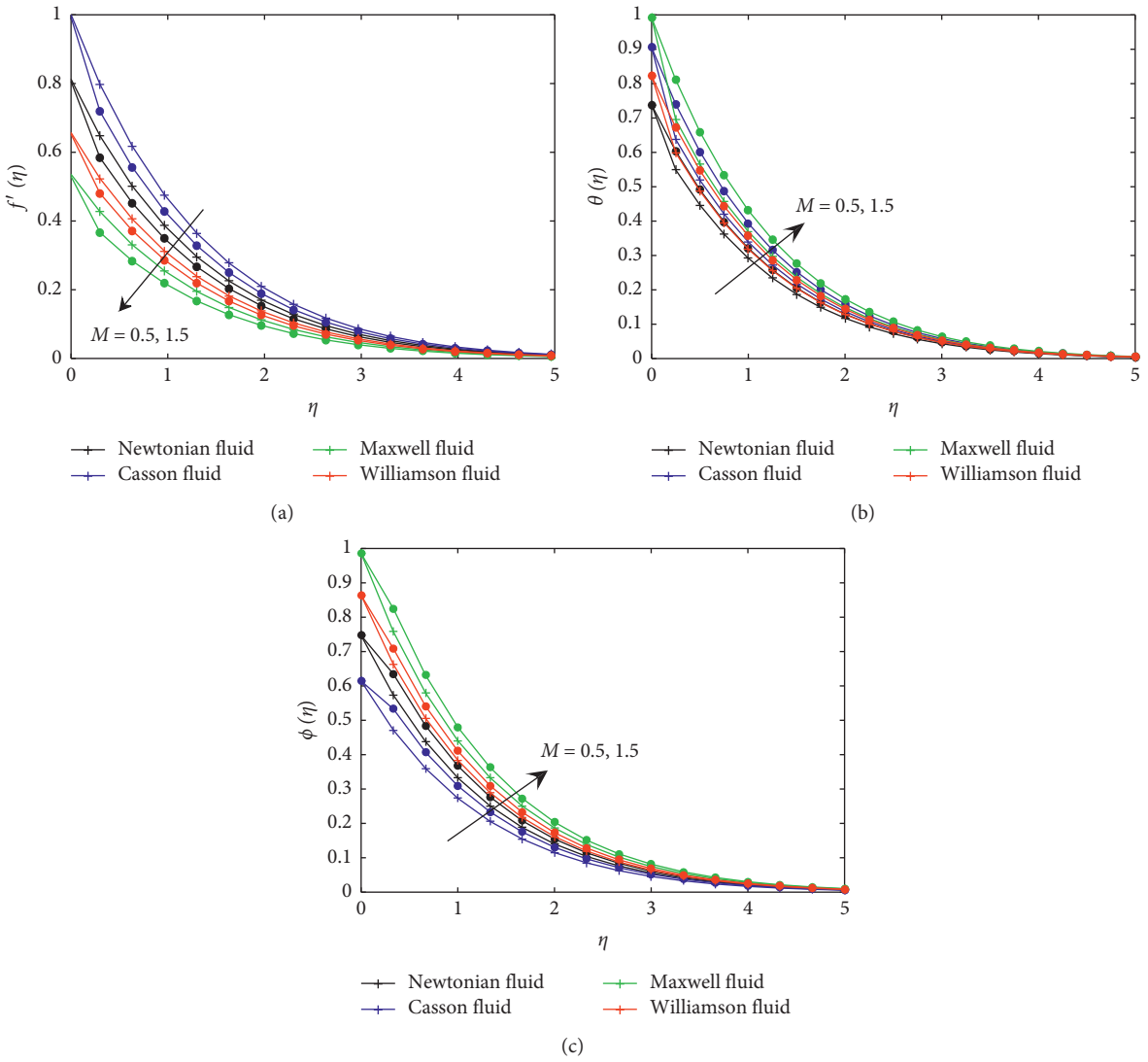

Figure 2: Effects of M for various fluid behavior: (a) $f'(\eta)$, (b) $\theta(\eta)$, and (c) $\phi(\eta)$.

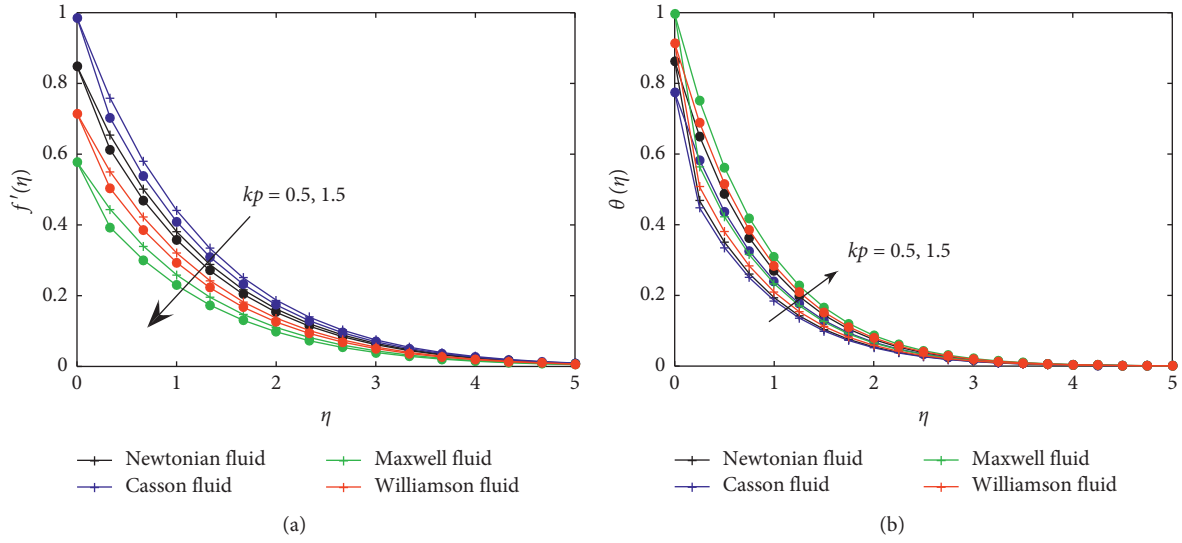

Figure 3: Continued.

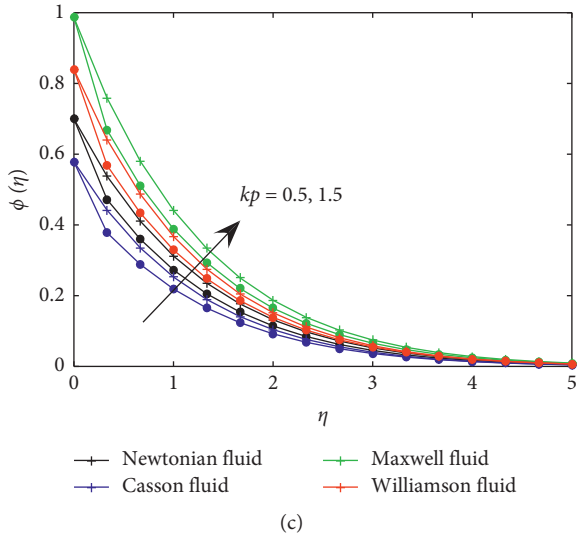

(c)

Figure 3: Effects of Kp for various fluid behavior: (a) $f'(\eta)$, (b) $\theta(\eta)$, and (c) $\phi(\eta)$.

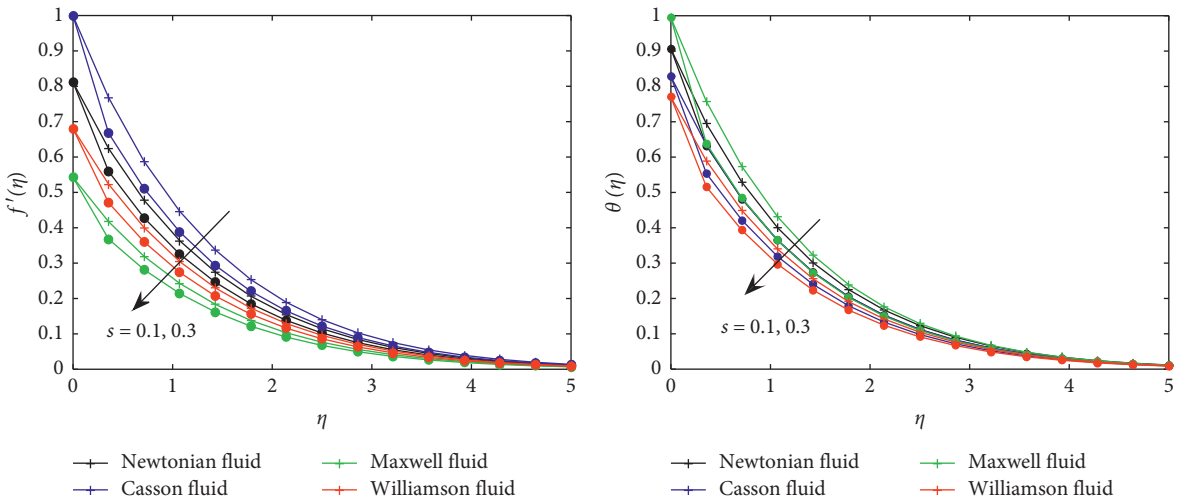

(a)

(b)

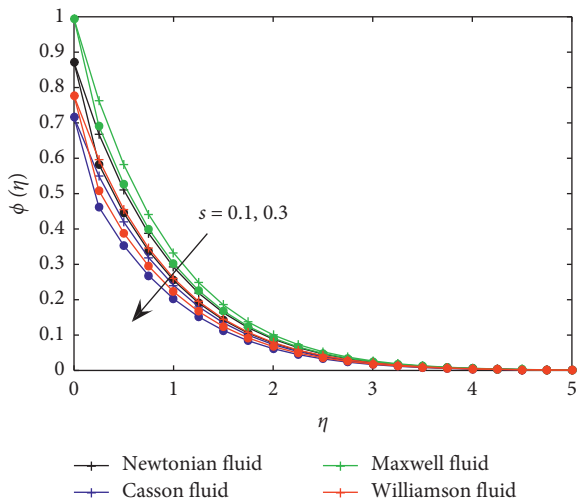

(c)

Figure 4: Effects of s for various fluid behavior: (a) $f'(\eta)$, (b) $\theta(\eta)$, and (c) $\phi(\eta)$.

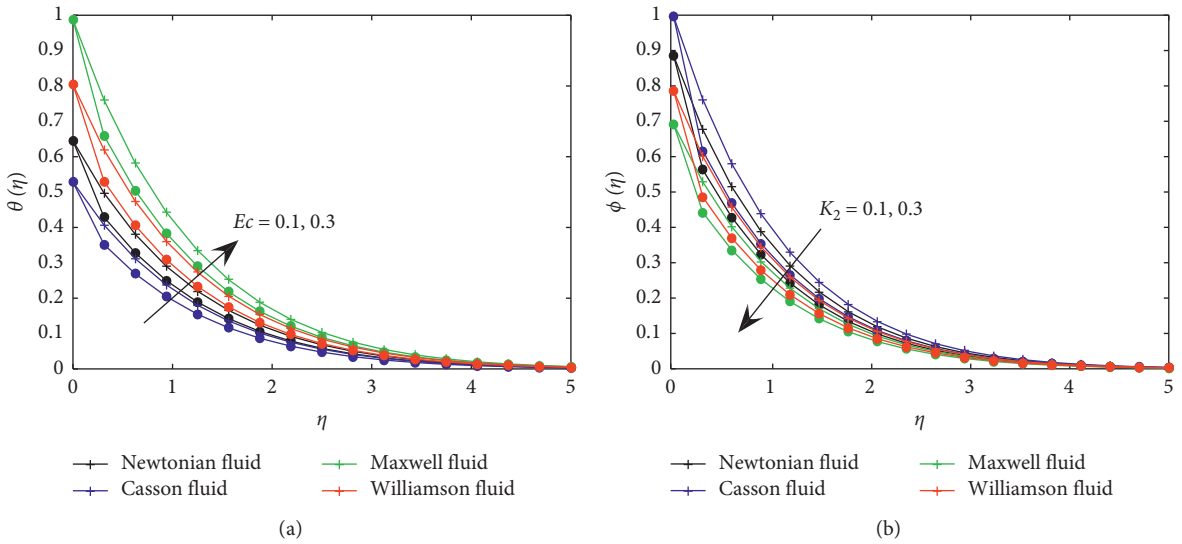

Figure 5: (a) Effects of *Ec* for various fluid behavior and (b) Effects of *K*2 for various fluids behavior.

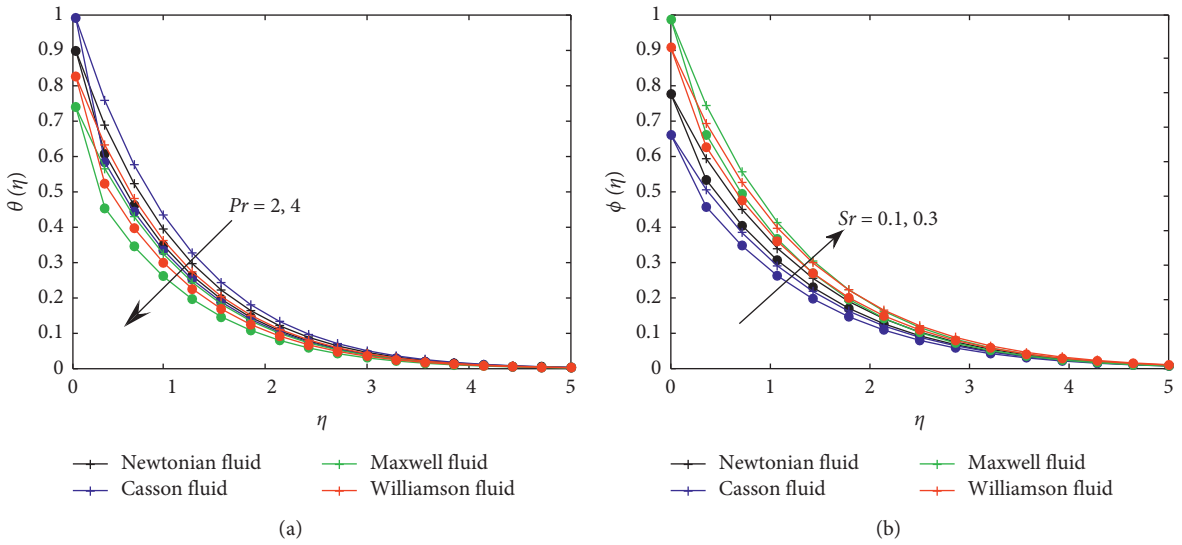

Figure 6: (a) Effects of *Pr* for various fluid behavior and (b) Effects of Sr for various fluids behavior.

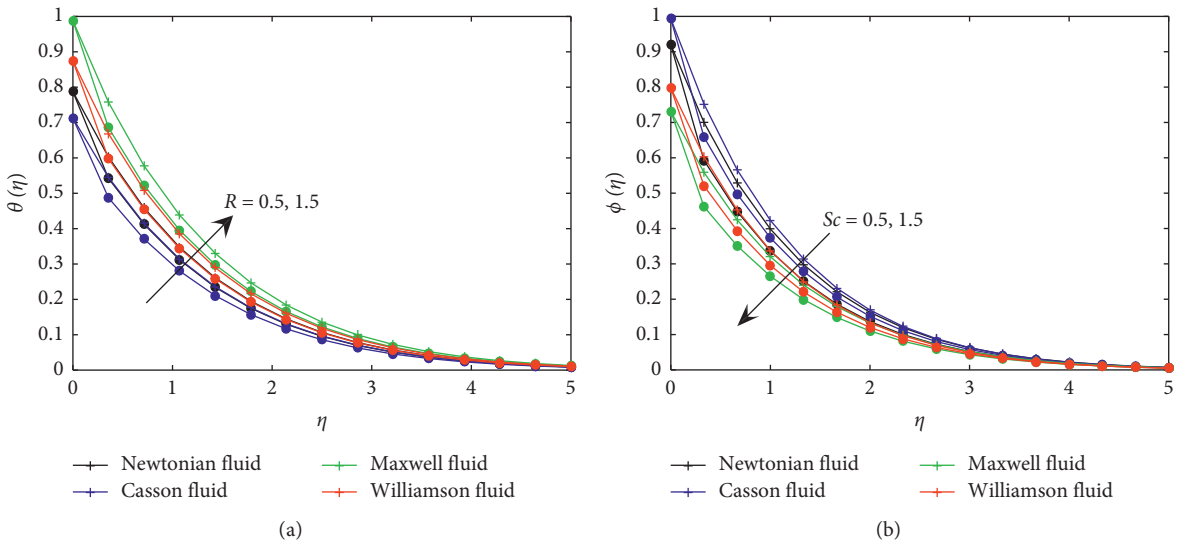

Figure 7: (a) Effects of *R* for various fluid behavior and (b) Effects of Sc for various fluids behavior..

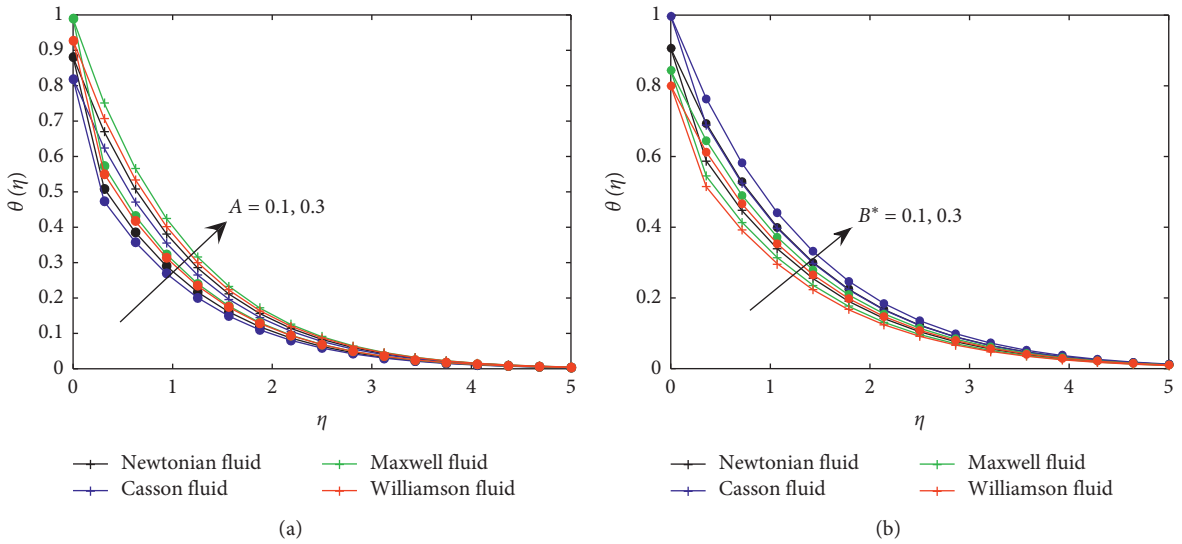

Figure 8: (a) Effects of A for various fluid behavior and (b) Effects of B^* for various fluids behavior.

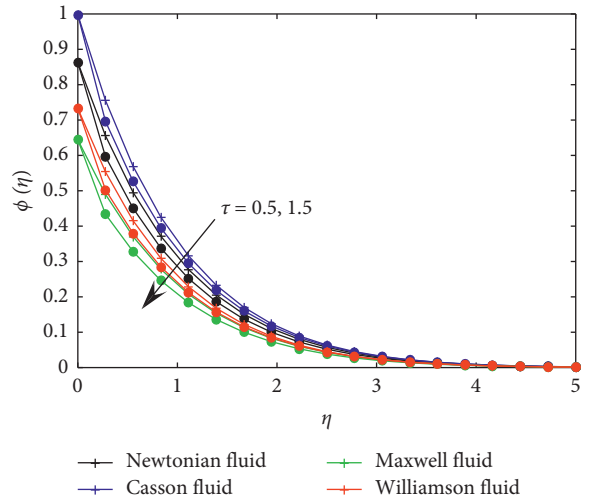

Figure 9: Effects of τ for various fluid behavior ($\phi(\eta)$).

Table 4: Comparison of skin friction coefficient, Nusselt number, and Sherwood number for Casson fluid for different values of auxiliary parameters.

M	Kp	s	Ec	R	Pr	A^*	B^*	K_2	Sr	Sc	τ	$-f''(0)$	$-\theta'(0)$	$-\phi'(0)$
0.5												1.248942869	0.5223705413	0.6519047716
1												1.405786382	0.4273428889	0.6134722537
1.5												1.547734561	0.3541449394	0.5858175883
	0.5											1.248942869	0.5223705413	0.6519047716
	1											1.405786382	0.4619143844	0.6166067357
	1.5											1.547734561	.3541449394	0.5858175883
		0.1										1.294677460	0.5603747092	0.6748160225
		0.2										1.248942869	0.5223705413	0.6519047716
		0.3										1.205324826	0.4893765453	0.6304308163
			0.1									1.248942869	0.6112442146	0.6608136057
			0.2									1.248942869	0.5223705413	0.6519047716
			.3									1.248942869	0.4286601580	0.6419888932

Table 4: Continued.

M	Kp	s	Ec	R	Pr	A^*	B^*	K_2	Sr	Sc	τ	$-f''(0)$	$-\theta'(0)$	$-\phi'(0)$
				0.5								1.248942869	0.5223705413	0.6519047716
				1								1.248942869	0.4230859062	0.6382072145
				1.5								1.248942869	0.3640244959	0.6305753245
					1							1.248942869	0.2232841158	0.6102780073
					2							1.248942869	0.5223705413	0.6519047716
					3							1.248942869	0.7823656402	0.6905963270
						0.1						1.248942869	0.5624243803	0.6519047716
						0.2						1.248942869	0.5223705413	0.6519047716
						0.3						1.248942869	0.4825058239	0.6467352497
							0.1					1.248942869	0.5825564064	0.6613382849
							0.2					1.248942869	0.5223705413	0.6519047716
							0.3					1.248942869	0.4825058239	0.6421579224
								0.1				1.248942869	0.5223705413	0.6035019859
								0.2				1.248942869	0.5223705413	0.6519047716
								0.3				1.248942869	0.5223705413	0.7000424843
									0.1			1.248942869	0.5223705413	0.6692940942
									0.2			1.248942869	0.5223705413	0.6519047716
									0.3			1.248942869	0.5223705413	0.6345310041
										0.5		1.248942869	0.5223705413	0.6519047716
										1		1.248942869	0.5223705413	1.061343186
										1.5		1.248942869	0.5223705413	1.402629301
											0.5	1.248942869	0.5223705413	0.6519047716
											1	1.248942869	0.5223705413	0.7559268839
											1.5	1.248942869	0.5223705413	0.8622851506

In Figures 8(a) and 8(b), A^* and B^* are plotted to know the nature of nonuniform positive heat source/sink parameter on temperature profile $\theta(\eta)$ which exhibits the increasing behavior of the temperature profile while increasing the value of A^* and B^*. It is noticed that the Maxwell fluid is highly influenced by A^*, while Casson fluid is more affected by the increased value of B^*. The positive values of A^* and B^* are responsible factors of heat generators, which release the heat energy to fluid flow, and this then causes to uplift the temperature profile. Figure 9 incorporates the effects of τ, i.e., thermophoretic parameter. It is observed that, by increasing the value of τ, the concentration species retards everywhere in the flow domain.

The effects of magnetic field, porosity, chemical reaction, radiation, heat source/sink parameters, and thermophoresis velocity and Schmidt, Soret, Eckert, and Prandtl numbers are described in Tables 1–4 for detailed intrinsic characteristics of Newtonian and non-Newtonian fluids. From Tables 1–4, we can conclude that increasing the magnetic field and porosity parameter leads to the enhancement of skin friction but reduces heat and mass flux rate, while slower down the rate of wall shear stress and heat and mass fluxes for suction/injection parameter. By rising values of skin friction $-f''(0)$, lessen the heat flux rate $-\theta(0)$ as more heat is absorbed; similarly, mass flux rate $-\phi(0)$ is also expected to reduce. Local Nusselt number was also seen to be decreased for larger values of Ec, R, A^*, and B^* but increases for rising values of Pr number, so it can be used as a cooling agent. The numerical outputs in the tables show the significant increment for mass flow rate as chemical reaction, thermophoresis, and Schmidt number increase. Obviously, these parameters have direct impact on the concentration profile. In these tables, it is evident that, by increasing the values of Ec, A^*, B^*, R, and Sr, the heat and mass flow rate decreases.

4. Conclusion

We have thoroughly investigated the behavior of velocity, temperature, and concentration profiles. The heat and mass transfer analysis has been performed theoretically via graphical and numerical approaches. This research describes the chemically reacting MHD flow in the porous medium for Newtonian and non-Newtonian fluids, namely, Maxwell, Williamson, and Casson fluids, over a stretching sheet under the effects of radiation, heat source, Soret, Schmidt, and Prandtl numbers. The semianalytical solutions have been obtained by using analytical methods such as ADM, HAM, and VIM. To tackle the unbounded domain, Pade approximation has been encountered. Some useful outcomes of the current study are listed as follows:

(i) Magnetic and porosity parameters (M and Kp) have the tendency to increase the heat and mass transfer rate, and Maxwell fluid is much appreciated but depreciates the velocity distributed, and here, Casson fluids dominate the other fluids when comparison is performed

(ii) Mass transfer rate continuously decreases for increasing trend of Schmidt number and chemical reaction parameter, and Casson fluid is intensively affected

(iii) Thermal and concentration profiles for Maxwell fluid are highly influenced as compared with other Newtonian and non-Newtonian fluids

(iv) Ec, Sr, R, and A^* enhance the thermal and concentration profiles, and Maxwell fluid has a dominating trend over other fluids

(v) Maxwell fluid has better heat and mass transfer tendency while compared with Newtonian, Williamson, and Casson fluids

(vi) The thermophoretic parameter τ is constantly working as an agent to increase the mass transfer rate and hence causes the reduction in concentration boundary layer thickness

Data Availability

The data used to support the findings of this study are included within the article.

Additional Points

(i) The comparison of MHD fluid flow in the porous medium over a stretching surface is studied; (ii) it is observed that Maxwell fluid dominates the other fluids when comparison is performed for heat and mass transfer; (iii) skin friction coefficient and heat and mass fluxes are obtained; (iv) the impact of suction, radiation, thermophoresis velocity, and internal heat source/sink is observed for various fluid categories; and (v) the effects of Prandtl number, Schmidt number, and chemical reaction reduce the thermal and concentration profiles.

Conflicts of Interest

The authors declare that they have no conflicts of interest.

References

[1] T. Hayat and M. Qasim, "Influence of thermal radiation and joule heating on MHD flow of a Maxwell fluid in the presence of thermophoresis," *International Journal of Heat and Mass Transfer*, vol. 53, no. 21-22, pp. 4780–4788, 2010.

[2] N. F. M. Noor, "Analysis for MHD flow of a Maxwell fluid past a vertical stretching sheet in the presence of thermophoresis and chemical reaction: World Academy of Science," *Engineering and Technology*, vol. 64, pp. 10–19, 2012.

[3] S. Shateyi, "A new numerical approach to MHD flow of a Maxwell fluid past a vertical stretching sheet in the presence of thermophoresis and chemical reaction," *Boundary Value Problems*, vol. 2013, no. 1, p. 196, 2013.

[4] T. Hayat, M. Awais, and A. Imtiaz, "Heat source/sink in a magneto-hydrodynamic non-Newtonian fluid flow in a porous medium: dual solutions," *PLoS One*, vol. 11, no. 9, 2016.

[5] F. M. Abbasi and S. A. Shehzad, "Heat transfer analysis for three-dimensional flow of Maxwell fluid with temperature dependent thermal conductivity: application of Cattaneo-Christov heat flux model," *Journal of Molecular Liquids*, vol. 220, pp. 848–854, 2016.

[6] M. S. Kumar, N. Sandeep, B. R. Kumar, and S. Saleem, "A comparative study of chemically reacting 2D flow of Casson and Maxwell fluids," *Alexandria Engineering Journal*, vol. 57, no. 3, pp. 2027–2034, 2018.

[7] M. Bilal, M. Sagheer, and S. Hussain, "On MHD 3D upper convected Maxwell fluid flow with thermophoretic effect using nonlinear radiative heat flux," *Canadian Journal of Physics*, vol. 96, no. 1, pp. 1–10, 2018.

[8] O. K. Koriko, T. Oreyeni, and O. A. Oyem, "On the analysis of variable thermophysical properties of thermophoretic viscoelastic fluid flow past a vertical surface with nth order of chemical reaction," *OALib*, vol. 5, no. 6, pp. 1–17, 2018.

[9] N. Sandeep and C. Sulochana, "Momentum and heat transfer behaviour of Jeffrey, Maxwell and Oldroyd-B nanofluids past a stretching surface with non-uniform heat source/sink," *Ain Shams Engineering Journal*, vol. 9, no. 4, pp. 517–524, 2018.

[10] B. A. Kumaria, K. R. Prasadb, and K. Kavitha, "Fully developed free convective flow of a Williamson fluid in a vertical channel under the effect of a magnetic field," *Advances in Applied Science Research*, vol. 3, no. 4, pp. 2492–2499, 2012.

[11] S. Nadeem, S. T. Hussain, and C. Lee, "Flow of a Williamson fluid over a stretching sheet," *Brazilian Journal of Chemical Engineering*, vol. 30, no. 3, pp. 619–625, 2013.

[12] S. Nadeem and S. T. Hussain, "Heat transfer analysis of Williamson fluid over exponentially stretching surface," *Applied Mathematics and Mechanics*, vol. 35, no. 4, pp. 489–502, 2014.

[13] T. Hayat, A. Shafiq, and A. Alsaedi, "Hydromagnetic boundary layer flow of Williamson fluid in the presence of thermal radiation and Ohmic dissipation," *Alexandria Engineering Journal*, vol. 55, no. 3, pp. 2229–2240, 2016.

[14] A. Parmar and S. Jain, "Comparative study of flow and heat transfer behavior of Newtonian and non-Newtonian fluids over a permeable stretching surface," *Global and Stochastic Analysis*, vol. 25, no. 1, pp. 41–50, 2017.

[15] K. A. Kumar, J. V. R. Reddy, V. Sugunamma, and N. Sandeep, "Simultaneous solutions for MHD flow of Williamson fluid over a curved sheet with nonuniform heat source/sink," *Heat Transfer Research*, vol. 50, no. 6, pp. 581–603, 2019.

[16] C. Raju, N. Sandeep, M. Ali, and A. Nuhait, "Heat and mass transfer in 3-D MHD Williamson-Casson fluids flow over a stretching surface with non-uniform heat source/sink," *Thermal Science*, vol. 23, no. 1, pp. 281–293, 2019.

[17] M. Mustafa, T. Hayat, I. Pop, and A. Aziz, "Unsteady boundary layer flow of a Casson fluid due to an impulsively started moving flat plate," *Heat Transfer-Asian Research*, vol. 40, no. 6, pp. 563–576, 2011.

[18] S. Nadeem, R. Ul Haq, and C. Lee, "MHD flow of a Casson fluid over an exponentially shrinking sheet," *Scientia Iranica*, vol. 19, no. 6, pp. 1550–1553, 2012.

[19] S. Nadeem, R. U. Haq, N. S. Akbar, and Z. H. Khan, "MHD three-dimensional Casson fluid flow past a porous linearly stretching sheet," *Alexandria Engineering Journal*, vol. 52, no. 4, pp. 577–582, 2013.

[20] S. Pramanik, "Casson fluid flow and heat transfer past an exponentially porous stretching surface in presence of thermal radiation," *Ain Shams Engineering Journal*, vol. 5, no. 1, pp. 205–212, 2014.

[21] N. Massarotti, "New benchmark solutions for transient natural convection in partially porous annuli"" *International Journal of Numerical Methods for Heat and Fluid Flow*, vol. 26, no. 3-4, pp. 1–55, 2016.

[22] C. Sumalatha and S. Bandari, "Effects of radiations and heat source/sink on a casson fluid flow over nonlinear stretching sheet," *World Journal of Mechanics*, vol. 5, no. 1, pp. 257–265, 2015.

[23] E. M. Arthur, I. Y. Seini, and L. B. Bortteir, "Analysis of casson fluid flow over a vertical porous surface with chemical reaction in the presence of magnetic field," *Journal of Applied Mathematics and Physics*, vol. 3, no. 6, pp. 713–723, 2015.

[24] H. R. Kataria and H. R. Patel, "Radiation and chemical reaction effects on MHD Casson fluid flow past an oscillating vertical plate embedded in porous medium," *Alexandria Engineering Journal*, vol. 55, no. 1, pp. 583–595, 2016.

[25] G. Patel and N. Sandeep, "Thermophoresis and Brownian moment effects on parabolic flow of MHD Casson and Williamson fluids with cross diffusion," *Journal of Molecular Liquids*, vol. 233, no. 1, pp. 262–269, 2017.

[26] C. S. K. Raju and N. Sandeep, "MHD slip flow of a dissipative Casson fluid over a moving geometry with heat source/sink: a numerical study," *Acta Astronautica*, vol. 133, no. 1, pp. 436–443, 2017.

[27] I. Ullah, S. Shafie, I. Khan, and K. L. Hsiao, "Brownian diffusion and thermophoresis mechanisms in Casson fluid over a moving wedge," *Results in Physics*, vol. 9, pp. 183–194, 2018.

[28] S. M. Hussain, R. Sharma, G. S. Seth, and M. R. Mishra, "Thermal radiation impact on boundary layer dissipative flow of magneto-nanofluid over an exponentially stretching sheet," *International Journal of Heat and Technology*, vol. 36, no. 4, pp. 1163–1173, 2018.

[29] N. S. Elgazery, "Nanofluids flow over a permeable unsteady stretching surface with non-uniform heat source/sink in the presence of inclined magnetic field," *Elgazery Journal of the Egyptian Mathematical Society*, vol. 27, no. 9, 2019.

[30] A. G. Madaki, R. Roslan, M. S. Rusiman, and C. S. K. Raju, "Analytical and numerical solutions of squeezing unsteady Cu and TiO_2-nanofluid flow in the presence of thermal radiation and heat generation/absorption," *Alexandria Engineering Journal*, vol. 57, no. 2, pp. 1033–1040, 2018.

[31] T. Murugesan and M. Dinesh Kumar, "Heat source/sink and chemical reaction effects on MHD and heat transfer flow of radiative nanofluid over a porous exponentially stretching sheet with viscous dissipation and ohmic heating," *International Journal of Basic Sciences and Applied Computing (IJBSAC)*, vol. 2, no. 7, 2019.

[32] T. Murugesan and M. Dinesh Kumar, "Effects of thermal radiation and heat generation on hydromagnetic flow of nanofluid over an exponentially stretching sheet in a porous medium with viscous dissipation," *World Scientific News*, vol. 128, no. 2, pp. 130–147, 2019.

[33] M. I. Anwar, M. Ali, K. Rafque, and S. A. Shehzad, "Soret-Dufour and radiative aspects in hydromagnetized nanofuid flow in stratifed porous medium," *SN Applied Sciences*, vol. 1, no. 11, p. 1430, 2019.

[34] M. A. Mjankwi, V. G. Masanja, E. W. Mureithi, and M. N. James, "Unsteady MHD flow of nanofluid with variable properties over a stretching sheet in the presence of thermal radiation and chemical reaction," *International Journal of Mathematics and Mathematical Sciences*, vol. 2019, Article ID 7392459, 14 pages, 2019.

[35] M. Venkateswarlu, P. Bhaskar, and D. V. Lakshmi, "Soret and Dufour effects on radiative hydromagnetic flow of a chemically reacting fluid over an exponentially accelerated inclined porous plate in presence of heat absorption and viscous dissipation," *Journal of the Korean Mathematical Society*, vol. 23, no. 3, pp. 157–178, 2019.

[36] M. Subhani and S. Nadeem, "Numerical analysis of micropolar hybrid nanofluid," *Applied Nanoscience*, vol. 9, no. 1, pp. 447–459, 2019.

[37] M. Kumar, G. J. Reddy, N. N. Kumar, and O. A. Bég, "Computational study of unsteady couple stress magnetic nanofluid flow from a stretching sheet with Ohmic dissipation," *Proceedings of the Institution of Mechanical Engineers, Part N: Journal of Nanomaterials, Nanoengineering and Nanosystems*, vol. 233, no. 2–4, pp. 49–63, 2019.

[38] K. Rafique, M. I. Anwar, M. Misiran et al., "Brownian motion and thermophoretic diffusion effects on micropolar type nanofluid flow with soret and dufour impacts over an inclined sheet: keller-box simulations," *Energies*, vol. 12, no. 21, p. 4191, 2019.

[39] K. Jabeen, M. Mushtaq, and R. M. Akram, "A comparative study of MHD flow analysis in a porous medium by using differential transformation method and variational iteration method," *Journal of Contemporary Applied Mathematics*, vol. 9, no. 2, 2019.

[40] K. Jabeen, M. Mushtaq, and R. M. Akram, "Analysis of the MHD boundary layer flow over a nonlinear stretching sheet in a porous medium using semianalytical approaches," *Mathematical Problems in Engineering*, vol. 2020, Article ID 3012854, 9 pages, 2020.

[41] A. Carotenuto, P. Marotta, N. Massarotti, A. Mauro, and G. Normino, "Energy piles for ground source heat pump applications, comparison of heat transfer performance for different design and operating parameters," *Applied Thermal Engineering*, vol. 124, pp. 1492–1504, 2017.